



OPEN ACCESS

EDITED BY

Kun Ji,
Hohai University, China

REVIEWED BY

Pengfei Dang,
Guangzhou University, China
Xiaodan Sun,
Southwest Jiaotong University, China
Yuxiang Tang,
King Abdullah University of Science and
Technology, Saudi Arabia

*CORRESPONDENCE

Mengtan Gao,
gaomt1957@163.com
Zongchao Li,
lizongchaigo@163.com
Jize Sun,
sun_jize@126.com

†PRESENT ADDRESS

Zhiwei Ji and Zongchao Li,
Minzu University, Beijing, China

SPECIALTY SECTION

This article was submitted to Structural
Geology and Tectonics,
a section of the journal
Frontiers in Earth Science

RECEIVED 27 October 2022

ACCEPTED 22 November 2022

PUBLISHED 13 January 2023

CITATION

Ji Z, Li Z, Sun J, Gao M, Li T, Huang T, Li N
and Guo X (2023), Estimation of
broadband ground motion
characteristics considering source
parameter uncertainty and
undetermined site condition in densely
populated areas of Pingwu.
Front. Earth Sci. 10:1081542.
doi: 10.3389/feart.2022.1081542

COPYRIGHT

© 2023 Ji, Li, Sun, Gao, Li, Huang, Li and
Guo. This is an open-access article
distributed under the terms of the
[Creative Commons Attribution License
\(CC BY\)](https://creativecommons.org/licenses/by/4.0/). The use, distribution or
reproduction in other forums is
permitted, provided the original
author(s) and the copyright owner(s) are
credited and that the original
publication in this journal is cited, in
accordance with accepted academic
practice. No use, distribution or
reproduction is permitted which does
not comply with these terms.

Estimation of broadband ground motion characteristics considering source parameter uncertainty and undetermined site condition in densely populated areas of Pingwu

Zhiwei Ji^{1†}, Zongchao Li^{1*†}, Jize Sun^{2*}, Mengtan Gao^{1*},
Tiefei Li¹, Ting Huang¹, Na Li¹ and Xiangyun Guo¹

¹Institute of Geophysics China Earthquake Administration, Beijing, China, ²Shenzhen Academy of Disaster Prevention and Reduction, Shenzhen, China

Three destructive earthquakes occurred in Pingwu and Songpan, Sichuan Province, China, between August 16 and 23, 1976. Due to the seismic monitoring capability at that time, the ground motion characteristics of these earthquakes are very vague. Realistic and reliable strong ground motion input plays an important role in seismic building design and urban-scale earthquake damage simulation. This study reproduces the main broadband ground motion characteristics of the 1976 Ms7.2 Songpan earthquake in densely populated areas of Pingwu. The empirical Green's function method and finite difference method are used to simulate high-frequency and low-frequency ground motion, respectively, and the broadband ground motion is obtained by superposition within the frequency range. In addition, in combination with the "Recipe" source parameter scheme, various uncertainties in the source parameters are considered, including the source mechanism, source depth, asperity parameters, etc. We obtain 36 kinds of broadband ground motion at six typical locations in the Pingwu area. Moreover, we test the rationality of the obtained broadband ground motion by ground motion prediction equations (GMPEs), and the broadband ground motions are consistent with the local ground motion characteristics. The results show broadband ground motions obtained from the scenario earthquake in this paper can meet the destructive capacity of earthquakes of this magnitude. The hybrid method can effectively compensate for the lack of long-period components of the original empirical Green function method. This research also proves that the peak ground acceleration (PGA) of ground motion is mainly contributed by high-frequency ground motion components. Long-period ground motion contributes most to the peak ground velocity (PGV), and about twice the contribution of high-frequency ground motion. Concerning the Chinese seismic intensity scale (GB/T 17742-2020) and China Seismic Ground Motion Parameter Zoning Map (GB18306-2015), the basic fortification intensity in the Pingwu area is VIII. In this paper, the seismic intensity of PWN is VI-VII, indicating that the buildings at this location are

less likely to be damaged after the earthquake. The seismic intensity of other regions is VII-IX and buildings are more likely to be damaged during the earthquake at these locations. There are many mountains and valleys in the Pingwu area, and the probability of landslides, debris flows, and other disasters after an earthquake is very high, and we should give special attention to the impact of secondary disasters caused by earthquakes. It is necessary to prevent dammed lakes and other disasters caused by landslides and debris flows.

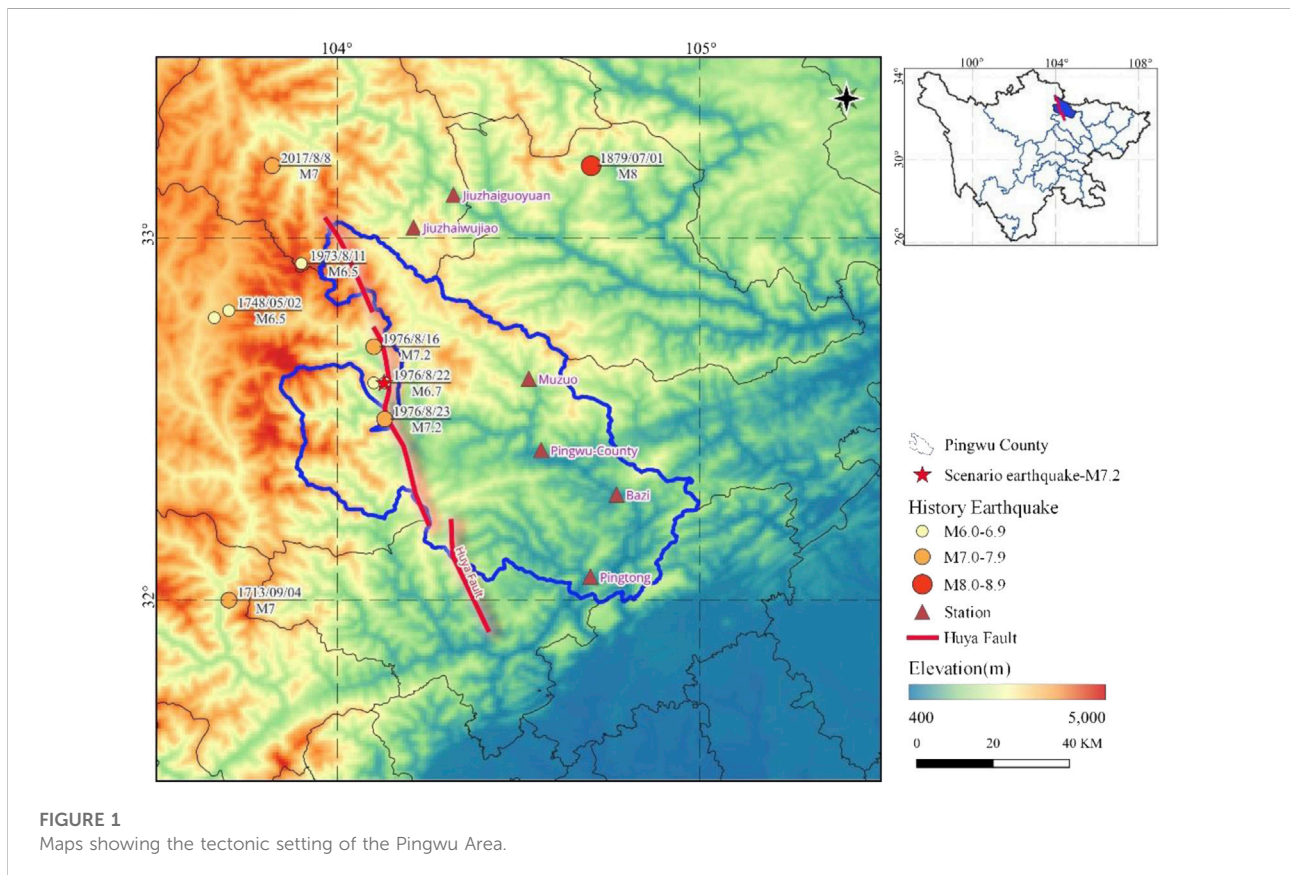
KEYWORDS

broadband ground motion, uncertainty, finite difference method, green function method, recipe scheme

Introduction

On August 16, 1976, an Ms7.2 earthquake occurred at the junction of Songpan County and Pingwu County, Sichuan Province, China. Another two earthquakes occurred successively in the following week: an Ms6.7 earthquake on August 22 and an Ms7.2 earthquake on August 23 (Figure 1). The seismogenic structures of the three earthquakes are the Huya fault (Figure 1) at the east boundary of the Minshan fault block, which is located northwest of the Longmenshan fault. As the east boundary of the Minshan fault block, the Huya fault is located in the transition zone from the Bayan Hara block to the Motianling block, belonging to the geomorphic boundary between the high

and middle mountains (Zhao et al., 1994; Zhou et al., 2006; Li et al., 2018). The Huya fault is also an important part of the compressional transformation tectonic system at the east end of the East Kunlun strike-slip fault (Kirby et al., 2007; Xu et al., 2008). Its seismic activity is frequent, and since historical records were initiated, many strong earthquakes with magnitudes of 6.0–7.2 have occurred along the boundary fault of the Minshan fault block. The Huya fault is located in the mountain valley area. Due to the limitation of traffic conditions, many scholars have different interpretations of its nature and segmentation. Some have reported that the Huya fault is a Quaternary thrust fault (Deng et al., 1994; Zhao et al., 1994), and some that the fault constitutes mainly strike slip with a thrust



nature (Jones et al., 1984; Zhou et al., 2006; Xu et al., 2008). The focal area of the Jiuzhaigou Ms7.0 earthquake in 2017 is located at the intersection of the Tazang, Minjiang and Huya faults (Xu et al., 2008), which shows that the Huya fault is still a strong active fault and that there is still the possibility of large earthquakes in the Songpan and Pingwu areas in the future.

Strong earthquakes in mountain and canyon areas are likely to cause a large number of secondary disasters in the region, such as mountain collapse, rockfall, and mud rock flow, causing severe casualties and economic losses. The Ms6.8 earthquake in Luding in 2022 was mainly associated with secondary disasters. The 1976 Songpan and Pingwu earthquake was one of the few successfully predicted earthquakes in history. Although it caused great damage to buildings, large casualties were prevented. With the development of the social economy, the economic losses caused by strong earthquakes are also increasing. Improving the seismic fortification level of buildings and improving the disaster prevention level of cities is one of the problems faced by seismic engineers and is an appropriate context for studying historical earthquakes. Because of limitations in earthquake-monitoring ability, most regions that have experienced strong earthquakes have failed to record the earthquake waveform to accurately characterize the characteristics of earthquake ground motion, which is unfortunate for most regions in the world that have experienced historical large earthquakes. To obtain a clearer understanding of the ground motion characteristics of these strong earthquakes and reduce the possible damage caused by future earthquakes, it is necessary to reproduce historical earthquakes using ground motion simulation methods.

For seismic analysis of lifeline projects and long-span structures, it is necessary to consider a wider frequency range of ground motion. Because the small-scale source information and the near-surface medium information are difficult to obtain, there is a large technical obstacle to directly simulate broadband ground motion. Therefore, the hybrid method of separately simulating low-frequency ground motion (<1 Hz) and high-frequency ground motion (>1 Hz) and superimposing them in the frequency domain is an effective means to obtain reasonable broadband ground motion. Graves and Pitarka (2010) combined a deterministic approach and a semistochastic approach to reproduce broadband ground motion of the Imperial Valley, Loma Prieta, Landers, and Northridge earthquakes. Thus far, the University of Southern California's Broadband Platform 22.4.0 platform (https://strike.scec.org/scecpedia/Broadband_Platform) has been used. A total of 9 broadband ground motion simulation schemes have been reported (Zeng et al., 1994; Motazedian and Atkinson, 2005; Graves and Pitarka, 2010; Mai et al., 2010; Schmides et al., 2010; Morikawa et al., 2011; Song, 2015; Iwaki et al., 2016a; Iwaki et al., 2016b; Pitarka et al., 2017). Three simulation schemes are based on the "Recipe" scheme proposed by Irikura and Miyake (2011), that is, the arrangement and combination of high-frequency and low-frequency ground motion obtained by the high-frequency and low-frequency

ground motion simulation method. The methods involved in the Recipe scheme include the frequency-wavenumber Green's function (FK method), Stochastic Finite-Fault method, finite difference method (FDM), and Stochastic method, etc. Hartzell et al. (1999) used the 3D finite difference method to calculate low-frequency ground motion and the Green function method to calculate high-frequency ground motion when investigating the broadband ground motion of the 1994 Northridge earthquake and evaluated the influence of different types of Green functions.

For long-period ground motion simulation, the finite element method is generally used, which can take into account the influence of complex geological structures such as terrain and basin. High-frequency ground motion simulation uses the empirical Green function method to simulate strong ground motion using small-earthquake records observed near the source area, which can effectively reproduce the ground motion characteristics of large earthquakes (Miyake et al., 2003). This method requires a sufficient number of small-earthquake records in the target area. Benefiting from China's increasingly improved earthquake-monitoring capability, we have obtained a large amount of earthquake-monitoring data and seismic waveforms in the Songping area, which gives us the opportunity to reproduce the seismic acceleration time history and corresponding seismic characteristics of the 1976 Songpan-Pingwu Ms7.2 earthquake at typical locations (densely populated areas, major project sites or lifeline project locations).

For the estimation of historical earthquakes, many parameters are uncertain, and uncertainties in the source and fault parameters affect the results of ground motion simulation (Atkinson and Beresnev, 2002; Aochi and Douglas, 2006; Sorensen et al., 2007; Causse et al., 2008; Graves et al., 2008; Ripperger et al., 2008; Wang et al., 2008; Ansal et al., 2009; Cultrera et al., 2010; Imperatori and Mai, 2012; Ji et al., 2022). Therefore, when simulating historical earthquakes, we focus on the uncertainty factors of many source parameters (such as asperity parameters, the source mechanism, and the initial rupture location), express the characteristics of ground motion with a reasonable range of values, and verify the reliability of ground motion evaluation results in combination with a variety of seismic attenuation relationships.

In this paper, the broadband ground motion simulation scheme is adopted to reproduce the ground motion characteristics of the 1976 Songpan Ms7.2 earthquake on the Huya fault at a typical location in the Pingwu area by focusing on multiple uncertainties in the source parameters. The empirical Green function is introduced based mainly on a large number of small-earthquake records recorded in the Songpan and Pingwu areas, which can take into account the rupture process of the source and the complexity of the propagation medium. The introduction of the finite difference method (FDM) is mainly due to its advantages of simple spatial discretization and high

computational efficiency. In addition, considering uncertainties in the source parameters, a broadband ground motion simulation scheme is developed to simulate historical earthquakes; reproduce their broadband ground motion characteristics; provide effective data support for the seismic design of major mega projects, lifeline projects, and other research fields that need input of ground motion parameters; and provide some reference for reducing the severity of possible earthquake disasters in the Pingwu region in the future.

Recipe scheme and simulation method

Recipe broadband ground motion simulation scheme

The Recipe scheme is an optimization scheme for predicting future scenario earthquakes based on the characteristic source model. The scheme focuses on the correlation between the inhomogeneity of the fault rupture surface and uncertainties in the asperity parameters on the ground motion prediction results. Based on the empirical relationship between source parameters, the parameters of source models used to predict ground motion are divided into three categories: external parameters, internal parameters and other parameters. The external parameters are defined as the total rupture area and the total seismic moment of the fault. The internal parameters are defined as the nonuniform slip at the source, the area of the asperity, the stress drop of each asperity, etc. The fracture nucleation and termination mode is an external fault parameter related to active fault landforms (Irikura and Miyake, 2011). In the Recipe scheme, there are two important factors for predicting strong earthquake ground motion: one is the source model of each scenario earthquake, and the other is the use of an appropriate Green's function from the source to the site. Finally, the validity of the results is confirmed by comparing the historical data with the predicted ground motion. Using the Recipe scheme to estimate future scenario earthquakes can provide reasonable strong ground motion characteristics for seismic engineers, government earthquake emergency response personnel, etc., to facilitate subsequent corresponding actions (Irikura and Miyake, 2011). The present paper refers to the ground motion simulation scheme of Irikura and Miyake (2011) and develops a broadband ground motion simulation scheme (Figure 2).

Ground motion simulation method

We use the FDM to simulate the low-frequency ground motion in this paper. Aoi and Fujiwara. (1999) proposed a

finite difference method based on discontinuous grids, which greatly improved the calculation efficiency on the premise of ensuring calculation accuracy. During the simulation of ground motion, the stratum medium is divided into grids of different thicknesses according to the depth, and the three-dimensional coordinates of the grids are given. The rupture area is set as the combination of finite sub faults, and the source parameters (slip, seismic moment, source time function) on the sub faults are calculated by difference to simulate the rupture process of the fault in the earthquake and then simulate the ground motion. This method can calculate the long-period ground motion of any three-dimensional heterogeneous medium structure and effectively simulate the long-period ground motion of complex geological structure areas such as fault zones and sedimentary basins (Iwaki and Iwata, 2010; Iwaki et al., 2016a; Luo et al., 2020). In this paper, the open source software Ground Motion Simulator (GMS) based on the discontinuous grid finite difference method is used to calculate the low-frequency part of broadband ground motion.

The empirical Green function method is used to simulate high-frequency ground motion in this paper. Hartzell (1978) first proposed this method, which mainly uses foreshock or aftershock records of large earthquakes as the Green function to synthesize large earthquakes. The source of a large earthquake is considered to be composed of a series of sub-earthquake sources, and an aftershock or foreshock record of appropriate size is selected as the Green function. A small earthquake is equivalent to a sub-earthquake. According to a certain rupture mode, these empirical Green functions are superposed to obtain the time history of the large earthquake ground motion. Irikura and Miyake et al. (Irikura and Kamae, 1994; Miyake et al., 2003; Irikura and Miyake, 2011) system proposed the idea of using empirical Green function method to simulate future ground motions, and verified the reliability of this method with several earthquake examples. They also summarized the general steps of the method to simulate ground motion. Through the continuous efforts of many scholars, the empirical Green function method has gradually developed into a relatively mature ground motion simulation method for strong earthquakes and has been widely recognized (Li et al., 2021, 2022).

After the low-frequency and high-frequency ground motion is simulated respectively, they are superimposed into broadband ground motion in the frequency domain. First, the two parts are filtered. The final frequency range of the high-frequency ground motion is 1–25 Hz, and the final frequency range of the low-frequency ground motion is 0.1–1.0 Hz. The high-frequency and low-frequency ground motion is superposed at a frequency of 1.0 Hz (Roten et al., 2012; Iwaki et al., 2016b), and the effective frequency band of the final broadband is 0.1–25.0 Hz (Figure 3).

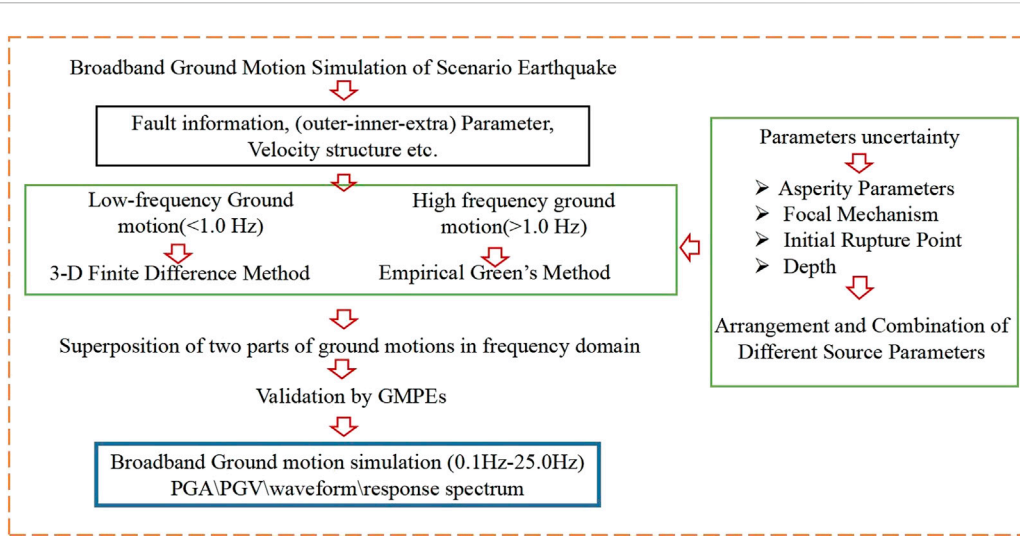


FIGURE 2
Flowchart of scenario earthquake broadband ground motion simulation in Pingwu Area.

Uncertainty in the source parameters

Uncertainties in the source parameters is the main factor to be considered in this study, arising mainly from uncertainties in the asperity parameters, the source mechanism, the source depth,

the initial rupture point. The empirical Green function method and the finite difference method are used to address uncertainties in these parameters. Some parameters used in the two different methods have some difference which are caused by the difference of reference source and

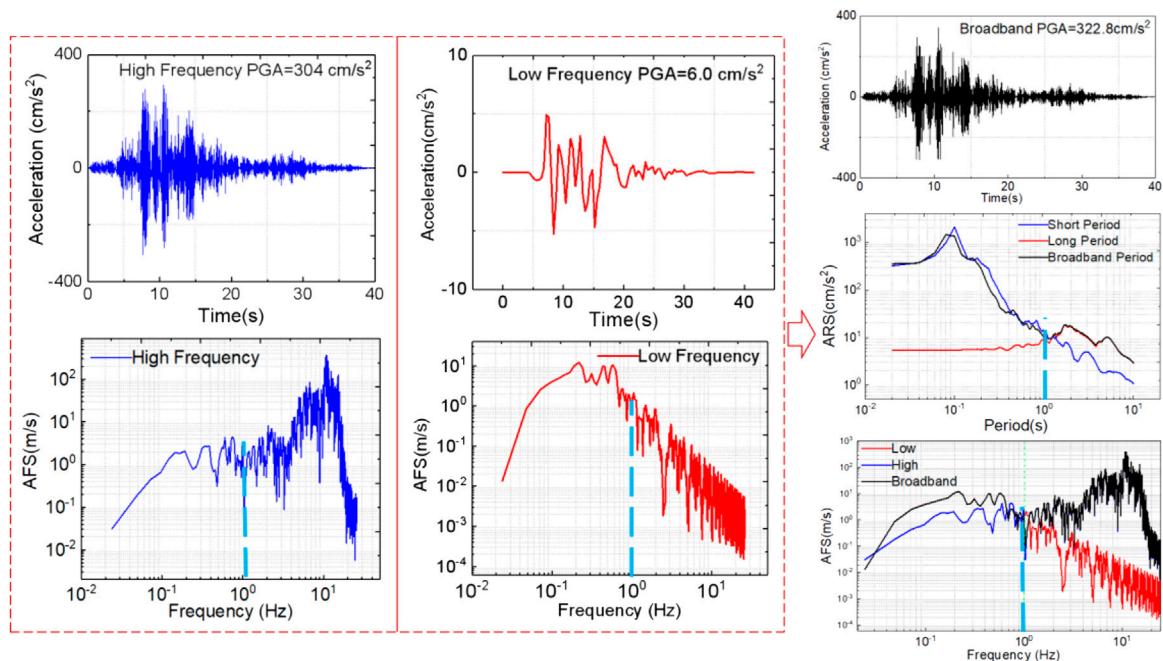


FIGURE 3
Schematic diagram of superposition of high-frequency and long-period ground motion waveforms in the frequency domain.

TABLE 1 Source parameters used by the finite difference method in the Pingwu scenario earthquake.

Source kinematics parameters	One asperity	Reference
Rupture area (km ²) = length (km)×width (km)	50 × 20	Wang, (2004)
Total seismic moment tensor M ₀ (N·m)	3.98e+19	Hanks and Kanamori, (1979)
Average slip of the asperity/background area (cm)	330/115	Somerville et al., 1999; Wang, 2004
Asperity area (km ²)	220	
M ₀ of the asperity/background area (N·m)	1.75e + 19/2.23e + 19	
Rise time of the asperity/background area (s)	2.987/1.493	Somerville et al. (1999)
Rupture velocity (km/s)	2.8	
Focal mechanism (strike/dip/rake)	340/Uncertainty/0	Tang and Liu, (1981)

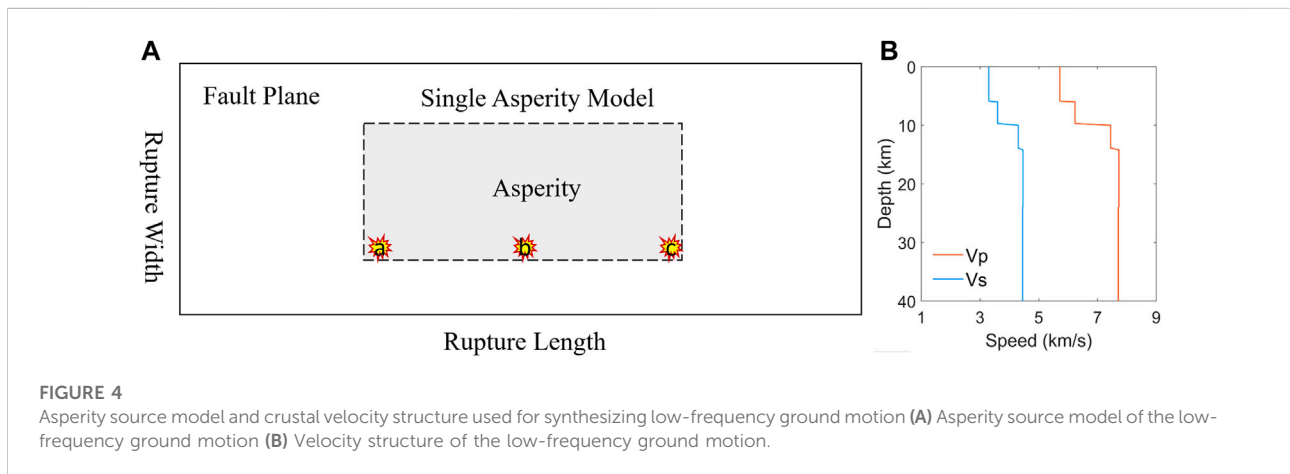


FIGURE 4 Asperity source model and crustal velocity structure used for synthesizing low-frequency ground motion (A) Asperity source model of the low-frequency ground motion (B) Velocity structure of the low-frequency ground motion.

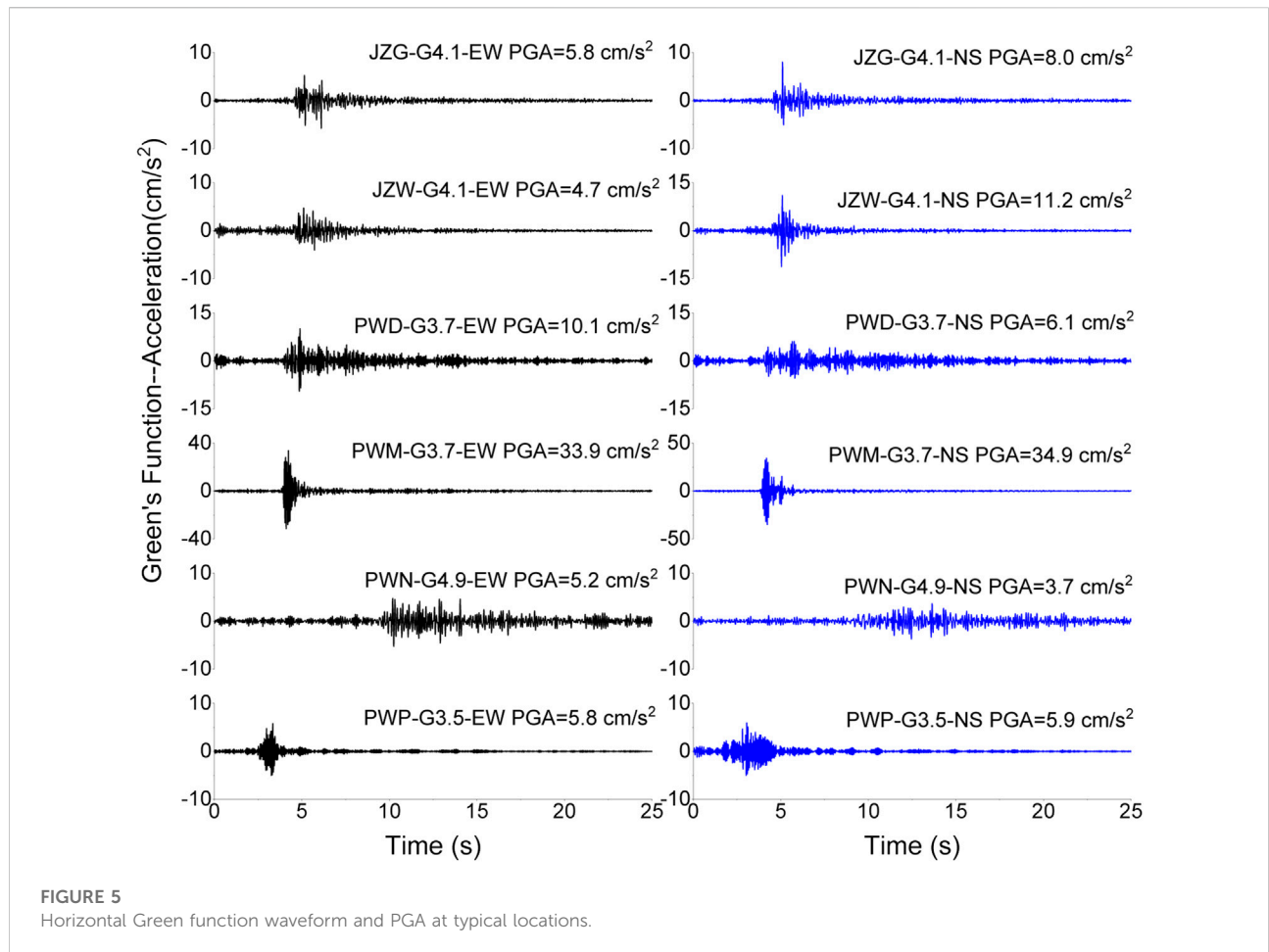
experience relationship, such as the seismic moment- M_0 (Hanks et al., 1978; Somerville et al., 1999). The results also show that the difference of these parameters has little influence on the characteristic of ground motion when simulating the scenario earthquakes.

In this paper, the steps to obtain broadband ground motion are as follows: 1) For the source models of high-

frequency and low-frequency ground motion, the uncertainties in the source parameters are considered for calculation; 2) We arrange and combine the obtained ground motion to obtain the documents required for merging broadband ground motion; and 3) the ground motion is spliced at the frequency of 1.0 Hz to output the broadband ground motion time history.

TABLE 2 Source parameters used in the empirical Green function method for Pingwu scenario earthquakes.

Source parameters		Reference
Magnitude	M _s 7.2	Tang and Liu, (1981)
Seismic moment (N·m)	7.08e+19	Somerville et al. (1999)
Source depth (km)	10/15/22	Tang and Liu, (1981)
Fault area (km ²)	60 × 30	Tang and Liu, (1981)
Asperity area (km ²)	28.3 × 14.2	Somerville et al. (1999)
Shear wave velocity (km/s)	3.5	Yao et al. (2019)
Focal mechanism	175°–45°/60°/75°–57°	Institute of Geophysics, China Earthquake Administration



The source model used in the finite difference method needs to define parameters such as the rupture size, seismic moment, rise time, source mechanism, and asperity parameters (number, area). The type of fault, rupture speed and position of the initial

rupture point affect the low-frequency ground motion. The uncertainty in these parameters should be taken into account when simulating low-frequency ground motion. The source parameters set for these ground motion in this paper are

TABLE 3 Key parameters of Green function taken at each typical location in the Pingwu scenario earthquake.

Minor earthquake magnitude	M3.5	M3.7	M4.9	M4.1
Stress drop ratio C of large and small earthquakes	1.96	1.96	1.96	1.96
Number of sub faults	43	34	9	22
Sub fault length × sub fault width	0.66 km×0.33 km	0.83 km×0.42 km	3.14 km×1.57 km	1.28 km×0.64 km

Note: The magnitude of small earthquakes used at each location is not fixed, and each small earthquake has corresponding key parameters for scenario earthquakes.

TABLE 4 Relative position of stations corresponding to calculation points.

Calculation position	Jiuzhai wujiao	Jiuzhai guoyuan	Pingwu	Muzuo	Bazi	Pingtong
Station NO.	JZW	JZG	PWD	PWM	PWN	PWP
Epicentral distance (km)	37.4	47.4	45.5	36.0	69.2	78.1
Azimuth (°)	8.4	16.0	116.7	87.9	119.4	137.8

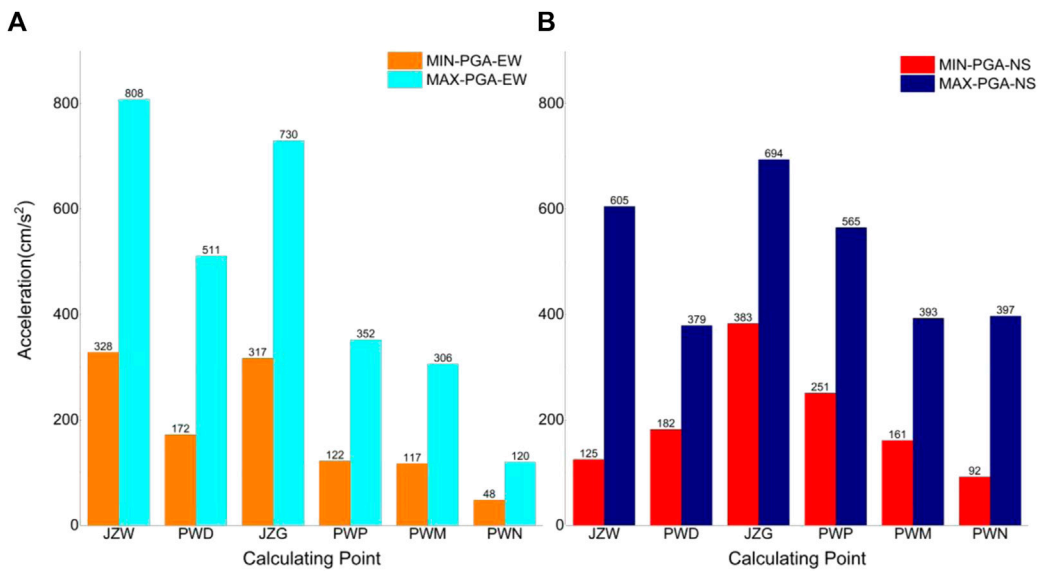


FIGURE 6 PGA value range of six typical locations. (A) Shows the PGA range of the EW component, (B) shows the PGA range of the NS component.

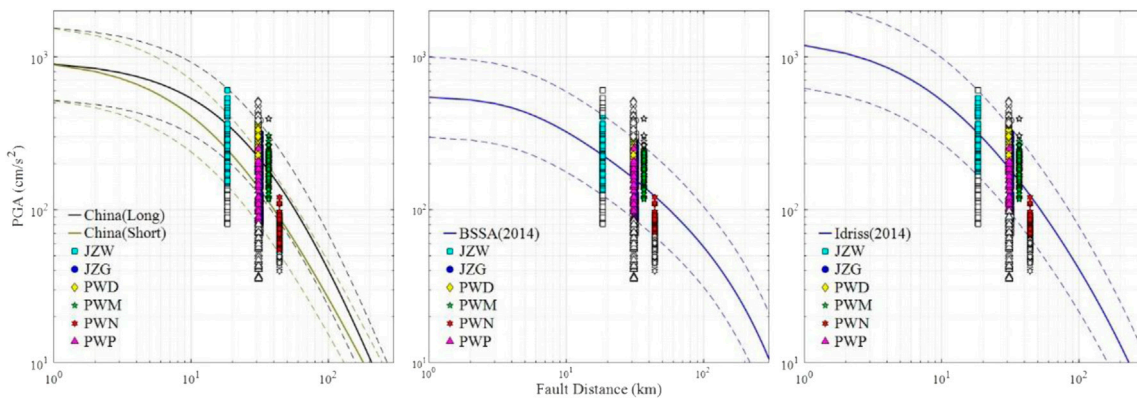


FIGURE 7 Acceleration time history of 6 calculation points selected by the three attenuation relationships.

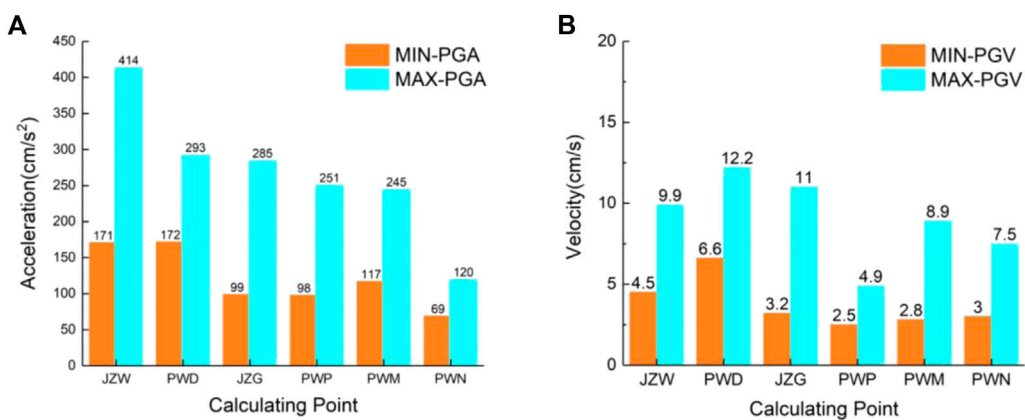


FIGURE 8 Value range of the PGA and PGV obtained from the intersection of the three types of attenuation relationships.

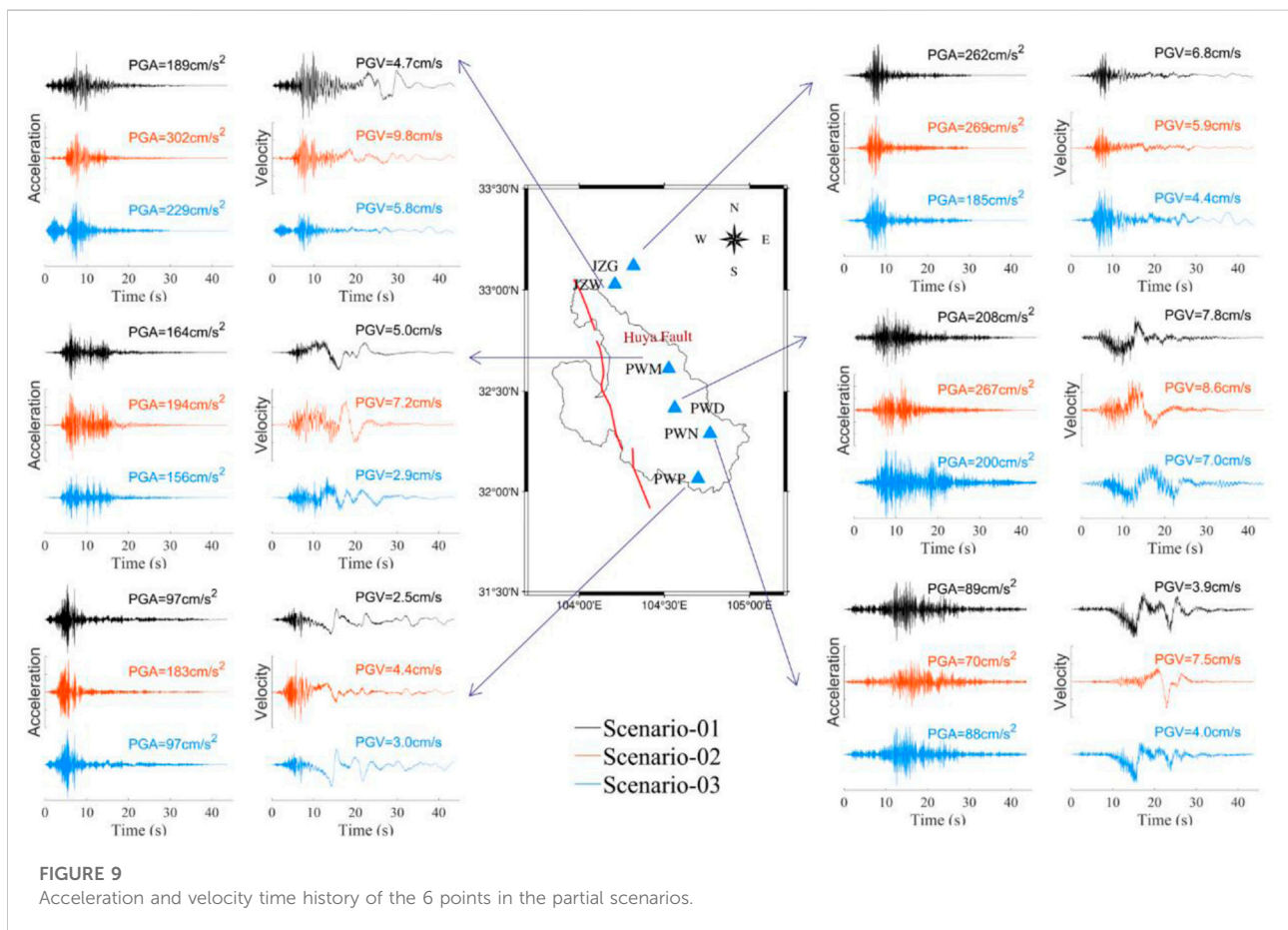
TABLE 5 Peak acceleration range of each typical position obtained after screening the three attenuation relationships.

GMPE	Range	PGA(cm/s ²)					
		JZW	JZG	PWD	PWM	PWN	PWP
BSSA (2014)	Max-PGA	414.37	285.35	293.07	245.00	120.39	250.79
	Min-PGA	126.01	86.33	171.72	117.00	68.62	87.76
Idris (2014)	Max-PGA	537.18	317.09	353.09	280.00	120.39	250.79
	Min-PGA	170.95	98.90	171.72	117.00	66.78	98.30
CN[China (GB18306-2015)]	Max-PGA	605.14	317.09	378.66	306.00	120.39	250.79
	Min-PGA	143.62	80.03	171.72	117.00	53.35	81.30

shown in Table 1. Among them, the parameter uncertainty includes the uncertainty in the fault dip angle and initial rupture point. The dip angles of the fault are 45°, 60°, and 75°, and the initial rupture point takes into account three uncertainties, as shown in Figure 4A. The rupture velocity is equal to 0.8Vs. (Somerville et al., 1999). The value of Vs. list in Table 2. In this paper, we calculate 36 scenario earthquakes. The finite difference method requires defining parameters related to

the crustal velocity structure, fault characteristics and seismic slip distribution (Luo et al., 2020). The crustal structure parameters used to calculate low-frequency ground motion in this paper are shown in Figure 4B (Long, 2008). The quality factor of each layer of the medium is calculated according to the empirical relationship proposed by Graves et al. (2008).

High-frequency ground motion arises mainly from near-fault ruptures, specifically associated with the asperity



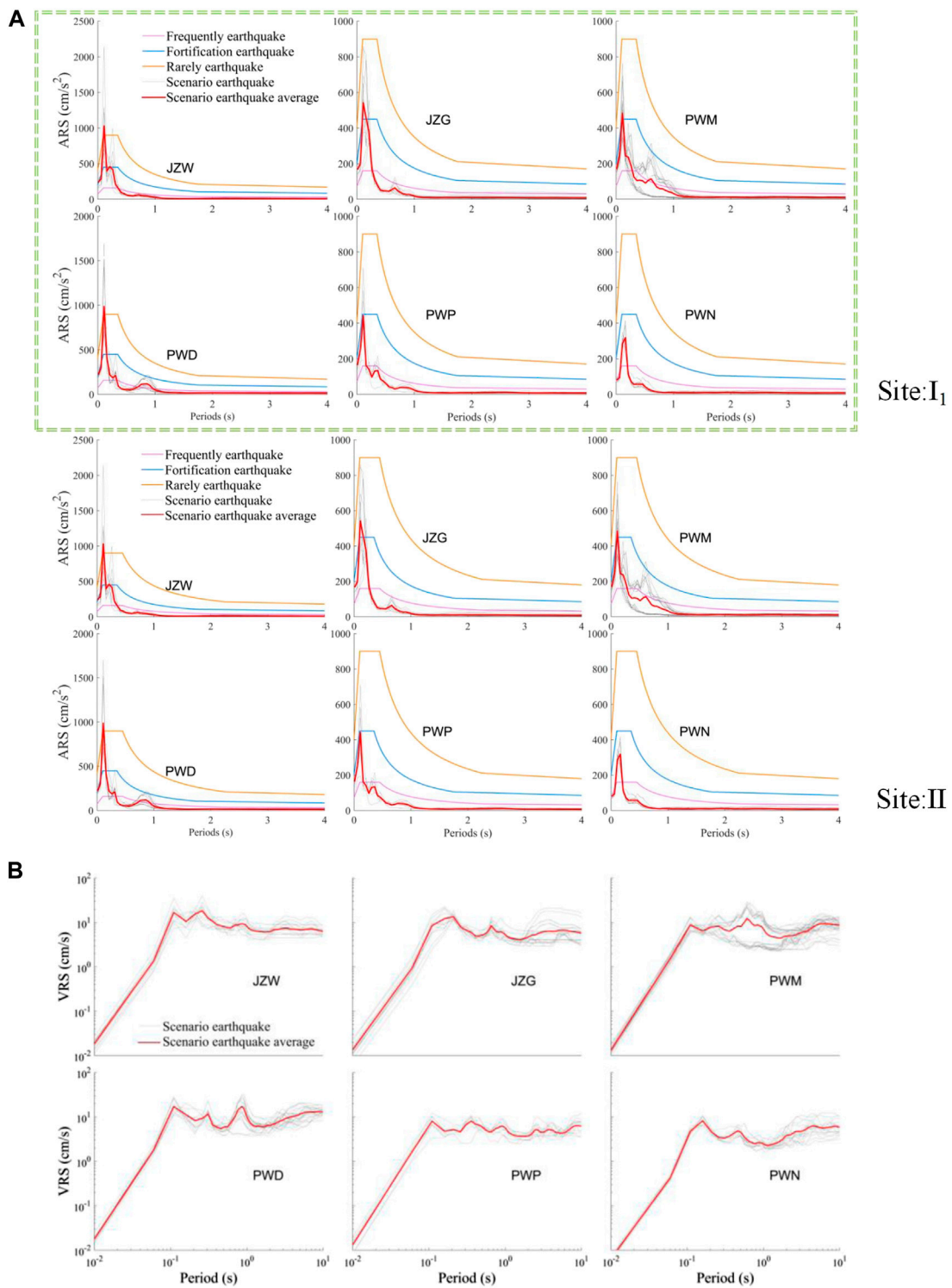


FIGURE 10 Acceleration response spectrum (A) and velocity response spectrum (B) of all scenarios in six typical locations (ARS stands for acceleration response spectrum, and VRS stands for velocity response spectrum).

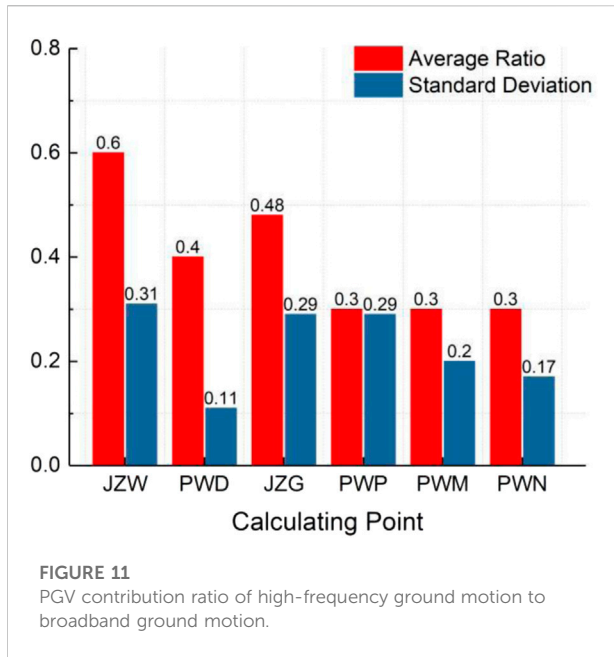


FIGURE 11
PGV contribution ratio of high-frequency ground motion to broadband ground motion.

parameters, initial rupture location, focal mechanism, and key focal parameters C (ratio of stress drop of large and small earthquakes) and N (Number of sub faults divided by the main earthquake fault plane). The parameter uncertainties mainly considered by the empirical Green function method in this paper include the parameter uncertainties in the asperity, source mechanism, initial rupture point, source depth, etc. For high-frequency earthquake ground motion simulations of scenario earthquakes, the initial exception point is generally selected from the bottom position of the asperity (Figure 4) (Miyake et al., 2003). The area of an asperity is 22% of the total fault area according to Somerville et al. (1999), and the total seismic moment of an asperity is 44% of the total seismic moment. The focal depth of the three historical large earthquakes of the 1976 Songpan Pingwu earthquake swarm (Tang and Liu, 1981) is selected as the focal depth. The focal mechanism is obtained from the focal mechanism database of the Institute of Geophysics, China Earthquake Administration, and uncertainty in the dip parameters is considered. The detailed parameters are shown in Table 3. We note here that there are differences in fault area and rupture area due to different output forms of low-frequency and high-frequency ground motion to the source model. In

addition, because the seismic moment of low-frequency and high-frequency ground motion are obtained from different statistical formulas, their values are different.

Broadband ground motion simulation results

In this paper, six typical locations are selected in Figure 1, and the broadband ground motion is estimated. These six points are places where the population density in the Pingwu area is relatively high or where major projects are located. In addition, these six regions have good small-earthquake records recorded by strong seismic stations (Table 4). The waveform of small earthquakes used in each typical location area is shown in Figure 5.

After fully considering various uncertainties in the source parameters, we calculated low-frequency and high-frequency ground motion of Ms7.2 scenario earthquakes in six typical locations in the Pingwu area. We selected low-frequency and high-frequency ground motion with the same source depth, number of asperities, and initial rupture point location to conduct broadband ground motion synthesis, and 36 kinds of broadband ground motion were obtained at each point.

Figure 6 shows the range of PGA values of broadband ground motion obtained from the arrangement and combination of two parts of ground motion at each typical location. The range of values for each location shown in the figure is large; for example, the difference between the maximum and minimum PGA at JZW is nearly 0.5 g, and in fact, not every scenario earthquake is appropriate. Therefore, we adopt the scheme commonly used worldwide and use a variety of GMPs to comprehensively determine the more reasonable broadband ground motion intensity range at each typical location. The GMPs mainly include the Fifth Generation Seismic Ground Motion Parameter Zoning Map of China (GB18306-2015) and NGA West2 (Boore et al., 2014; Idriss, 2014) attenuation relationship. We screened the broadband ground motion under different scenarios from the perspective of ground motion attenuation characteristics (Figure 7) and ultimately obtained more reasonable peak acceleration ranges for each typical location, as shown in Table 5. To obtain a more accurate and detailed range of the peak acceleration (Figure 8A) and peak velocity (Figure 8B) of broadband ground motion at six typical locations at the calculation points, we took the

TABLE 6 Corresponding intensity range of six typical locations in the Chinese seismic intensity scale.

Station name	JZW (cm/s ²)	JZG (cm/s ²)	PWD (cm/s ²)	PWM (cm/s ²)	PWN (cm/s ²)	PWP (cm/s ²)
Max-PGA	414	285	293	245	120	251
Min-PGA	171	99	172	117	69	98
Intensity scale	VII-IX	VII-VIII	VII-VIII	VII-VIII	VI-VII	VII-VIII

intersection of the range of three types of attenuation relations (Figure 8).

Finally, after screening, we obtained 220 broadband ground motion in 6 typical locations. Figure 9 shows partial broadband acceleration time histories and velocity time histories for six typical locations. Different coloured lines represent broadband ground motion under different scenarios. Limited by the length of the article, only the time histories of three scenarios are given for each typical location, and broadband ground motion of other scenarios are given as annexes. The acceleration spectrum and velocity spectrum can provide good data support for seismic design and seismic damage analysis of buildings. Figure 10 shows the acceleration response spectrum (ARS) (Figure 10A) and velocity response spectrum (VRS) (Figure 10B) of broadband ground motion obtained at six typical locations. The grey features represent the acceleration spectrum and velocity spectrum of the scenario earthquake, and the red line represents the average value of the acceleration spectrum and velocity spectrum. The acceleration spectrum contains two site conditions (Code for seismic design of buildings, GB 500101-2010):I₁ and II. Frequently earthquake, Fortification earthquake and Rarely earthquake in Figure 10A) stand for specification spectrum of Code for seismic design of buildings (GB 500101-2010). Red line represent average response spectrum (acceleration and velocity) of scenario earthquake. The six typical locations in this paper include the city of Pingwu with a large population density, scenic spots with a large pedestrian flow, and important traffic projects (Muzuo, Bazi, Pingtong) (Table 4). In typical locations JZW and PWD, the average acceleration spectrum of scenario earthquake are exceed rarely earthquake specification spectrum.

According to the PGA value range shown in Figure 8A, corresponding to the provisions of the China Seismic Intensity Scale (GB/T 17742-2020), the corresponding seismic intensities of six typical locations are shown in Table 6. With reference to the fortification requirements of the Fifth Generation Seismic Ground Motion Parameter Zoning Map of China (GB18306-2015), the basic fortification intensity in the Pingwu area is VIII. In the results of this paper, the PGA range at the PWN location is 69 cm/s²-120 cm/s², and the corresponding intensity is VI - VII, indicating that the buildings at this location were less likely to be damaged after the Ms7.2 earthquake. The PGA range at the JZW location is 171 cm/s²-414 cm/s², and the seismic intensity reaches IX. The site is likely to have been damaged during the earthquake. The PGA range of other locations is 98 cm/s²-251 cm/s², and the seismic intensity is VII-VIII. In mountainous and canyon areas such as Pingwu, the probability of landslides and debris flows occurring after the earthquake is very high. Special attention should be given to the impact of secondary disasters caused by the earthquake, especially the Fujiang River system flowing through Pingwu. It is necessary to prevent barrier lakes caused by landslides and debris flows. In practical application, if more detailed information about the site conditions can be

obtained, it is recommended that the results in this paper should be appropriately corrected.

Upon estimating the characteristics of broadband ground motion at six typical locations, this paper also summarizes the characteristics of the synthesized broadband ground motion. The peak ground acceleration of broadband ground motion is mainly contributed by high-frequency ground motion; that is, the energy released from the asperity area accounts for most of the energy of this earthquake, while the long-period ground motion contributes less to the peak ground acceleration. However, in terms of peak ground velocity, it is mainly contributed by long-period ground motion, which account for approximately 60%–70% of the PGV (typical locations: PWD, PWP, PWM, PWN), and high-frequency ground motion accounts for approximately 30%–40% of the PGV (Figure 11). This study also shows that the expression of different physical parameters by the long-period and high-frequency spectrum components of the synthesized broadband ground motion is quite different. Therefore, when selecting the simulation method to synthesize broadband ground motion, a reasonable simulation scheme should be selected according to the actual needs.

Conclusion and discussion

By considering multiple uncertainties in the source parameters, based on the Recipe scheme, combined with the finite difference method and empirical Green function method, we obtained the acceleration time history, velocity time history, and corresponding PGA, PGV, and response spectrum of broadband ground motion of the Pingwu Ms7.2 scenario earthquake. We use GMPEs to screen the obtained broadband ground motion, providing broadband ground motion within the reasonable range of 6 typical locations. The conclusions of this paper are as follows:

- (1) The broadband ground motion synthesis scheme adopted in this paper combines the advantages of low-frequency and high-frequency ground motion simulation methods, makes up for the shortcomings of the simple empirical Green function method in the context of long-period ground motion, and resolves the limitations of the finite difference method for calculating high-frequency ground motion.
- (2) High-frequency ground motion is the main PGA contributor; that is, the PGA of high-frequency ground motion is almost equal to the PGA of broadband ground motion, while high-frequency and long-period ground motion strongly contribute to the PGV, of which the contribution value of high-frequency ground motion is approximately 30%–40% and the contribution of long-period ground motion to the PGV is larger as a whole.
- (3) This study also shows that it is feasible to obtain the ground motion with a reasonable value range based on the research scheme of the source parameters of the Recipe scheme, and the ground motion with a reasonable value

range is also the best scheme to describe the scenario earthquake results.

- (4) In the most densely populated county, Pingwu County, the ground motion PGA range is approximately 170–290 cm/s², and the seismic intensity is approximately VIII. It is recommended that local people note these factors and take more practical and specific long-term earthquake prevention and disaster reduction measures.

Synthesizing the characteristics of ground motion in areas lacking large earthquake records is of great significance for local seismic design and earthquake disaster prevention. In many regions where historical earthquakes have occurred or where future earthquakes may occur, due to the lack of support from seismic records, the seismic input of other regions can be used only for the seismic design of buildings and earthquake damage simulation of buildings, which makes it difficult to truly express the actual seismic characteristics of the region. The work in this paper is intended to compensate for this shortcoming. In future earthquake research, it will be necessary to select more refined standards to determine the range of ground motion values and then screen out more appropriate ground motion. In the future, we plan to synthesize more representative broadband ground motion at typical locations, which will increase the reference value of this work.

Data availability statement

The raw data supporting the conclusion of this article will be made available by the authors, without undue reservation.

Author contributions

(First Author–JZ): Methodology, data curation, formal analysis, investigation, validation, writing-original draft, writing-review, editing. (Co-First Author and Corresponding Author–LZ): Conceptualization, methodology, data curation,

formal analysis, investigation, validation, writing-original draft, writing-review, editing. (Co-Corresponding Author–SJ): Writing-Original draft, writing-review draft, editing; Investigation; editing (Co-Corresponding Author–GM): Conceptualization; Methodology. (LT): editing. (HT): editing. (LN): editing, resource. (GX): resource.

Funding

This work was jointly supported by the Youth Fund of the National Natural Science Foundation (42104053) and the Research Project Fund of the Institute of Geophysics, China Earthquake Administration (DQJB22B21, DQJB22R30).

Acknowledgments

We would like to express our thanks to the Institute of Engineering Mechanics of China Earthquake Administration for providing the CENC seismic data. We also thank two reviewers and the editor-in-chief and associate editors for their careful reading and valuable suggestions.

Conflict of interest

The authors declare that the research was conducted in the absence of any commercial or financial relationships that could be construed as a potential conflict of interest.

Publisher's note

All claims expressed in this article are solely those of the authors and do not necessarily represent those of their affiliated organizations, or those of the publisher, the editors and the reviewers. Any product that may be evaluated in this article, or claim that may be made by its manufacturer, is not guaranteed or endorsed by the publisher.

References

- Ansal, A., Akinci, A., Cultrera, G., Erdik, M., Pessina, V., Tönük, G., et al. (2009). Loss estimation in Istanbul based on deterministic earthquake scenarios of the marmara sea region (Turkey). *Soil Dyn. Earthq. Eng.* 29, 699–709. doi:10.1016/j.soildyn.2008.07.006
- Aochi, H., and Douglas, J. (2006). Testing the validity of simulated strong ground motion from the dynamic rupture of a finite fault, by using empirical equations. *Bull. Earthq. Eng.* 4, 211–229. doi:10.1007/s10518-006-0001-3
- Aoi, S., and Fujiwara, H. (1999). 3D finite-difference method using discontinuous grids. *Bull. Seismol. Soc. Am.* 89, 918–930. doi:10.1785/BSSA0890040918
- Atkinson, G. M., and Beresnev, I. A. (2002). Ground motions at Memphis and St. Louis from M7.5–8.0 earthquakes in the new Madrid seismic zone. *Bull. Seismol. Soc. Am.* 92, 1015–1024. doi:10.1785/0120010203
- Boore, D. M., Stewart, J. P., Seyhan, E., and Atkinson, G. M. (2014). NGA-West2 equations for predicting pga, pgv, and 5% damped psa for shallow crustal earthquakes. *Earthq. Spectra* 30, 1057–1085. doi:10.1193/070113EQS184M
- Causse, M., Cotton, F., Cornou, C., and Bard, P.-Y. (2008). Calibrating median and uncertainty estimates for a practical use of empirical Green's functions technique. *Bull. Seismol. Soc. Am.* 98, 344–353. doi:10.1785/0120070075
- Cultrera, G., Cirella, A., Spagnuolo, E., Herrero, A., Tinti, E., and Pacor, F. (2010). Variability of kinematic source parameters and its implication on the choice of the design scenario. *Bull. Seismol. Soc. Am.* 100, 941–953. doi:10.1785/0120090044
- Deng, Q., Du, S., and Zhao, X. (1994). Tectonics, scismicity and dynamics of Longmenshan mountains and its adjacent regions. *Seismol. Geol.* 04, 389–403. (in Chinese).

- Gao, M., Chen, G., Xie, F., Xu, X., Li, X., Yu, Y., et al. (2015). *Seismic ground motion parameters zonation map of China: GB18306-2015*. Beijing: Beijing Standards Press of China, 173. (in Chinese).
- Geller, R. J. (1976). Scaling relations for earthquake source parameters and magnitudes. *Bull. Seismol. Soc. Am.* 66, 1501–1523. doi:10.1785/BSSA0660051501
- Graves, R. W., Aagaard, B. T., Hudnut, K. W., Star, L. M., Stewart, J. P., and Jordan, T. H. (2008). Broadband simulations for Mw7.8 southern san andreas earthquakes: Ground motion sensitivity to rupture speed. *Geophys. Res. Lett.* 35, L22302. doi:10.1029/2008GL035750
- Graves, R. W., and Pitarka, A. (2010). Broadband ground-motion simulation using a hybrid approach. *Bull. Seismol. Soc. Am.* 100, 2095–2123. doi:10.1785/0120100057
- Hanks, T. C., and Kanamori, H. (1979). A moment magnitude scale. *J. Geophys. Res.* 84, 2348–2350. doi:10.1029/JB084iB05p02348
- Hartzell, S., Harmsen, S., Frankel, A., and Larsen, S. (1999). Calculation of broadband time histories of ground motion: Comparison of methods and validation using strong-ground motion from the 1994 Northridge earthquake. *Bull. Seismol. Soc. Am.* 89, 1484–1504. doi:10.1785/BSSA0890061484
- Hartzell, S. H. (1978). Earthquake aftershocks as green's functions. *Geophys. Res. Lett.* 5, 1–4. doi:10.1029/GL005i001p00001
- Huang, S., Wang, Y., Dai, G., Fu, G., Luo, K., Li, X., et al. (2015). *Code for seismic design of buildings: GB50011-2010*. Beijing: China Architecture Building Press, 33. (in Chinese).
- Idriss, I. M. (2014). An NGA-West2 empirical model for estimating the horizontal spectral values generated by shallow crustal earthquakes. *Earthq. Spectra* 30, 1155–1177. doi:10.1193/070613EQS195M
- Imperatori, W., and Mai, P. M. (2012). Sensitivity of broad-band ground-motion simulations to earthquake source and Earth structure variations: An application to the messina straits (Italy). *Geophys. J. Int.* 188, 1103–1116. doi:10.1111/j.1365-246X.2011.05296.x
- Irikura, K., and Kamae, K. (1994). Estimation of strong ground motion in broad-frequency band based on seismic source scaling model and an empirical green's function technique. *Ann. Geophys.* 37.
- Irikura, K., and Miyake, H. (2011). Recipe for predicting strong ground motion from crustal earthquake scenarios. *Pure Appl. Geophys.* 168, 85–104. doi:10.1007/s00024-010-0150-9
- Iwaki, A., Fujiwara, H., and Aoi, S. (2016b). Broadband ground-motion simulation based on the relationship between high- and low-frequency acceleration envelopes: Application to the 2003 Mw 8.3 tokachi-oki earthquake. *Bull. Seismol. Soc. Am.* 106, 632. doi:10.1785/0120150273
- Iwaki, A., and Iwata, T. (2010). Simulation of long-period ground motion in the osaka sedimentary basin: Performance estimation and the basin structure effects. *Geophys. J. Int.* 181, 1062–1076. doi:10.1111/j.1365-246X.2010.04556.x
- Iwaki, A., Maeda, T., Morikawa, N., Miyake, H., and Fujiwara, H. (2016a). Validation of the recipe for broadband ground-motion simulations of Japanese crustal earthquakes. *Bull. Seismol. Soc. Am.* 106, 2214. doi:10.1785/0120150304
- Ji, Z., Li, Z., Chen, X., Li, T., Wu, Q., Zhang, B., et al. (2022). Uncertainties in prediction of near-fault long-period ground motion: An application to the 1970 tonghai earthquake (Ms7.8). *Pure Appl. Geophys.* 179, 2637–2660. doi:10.1007/s00024-022-03094-w
- Jones, L. M., Han, W., Hauksson, E., Jin, A., Zhang, Y., and Luo, Z. (1984). Focal mechanisms and aftershock locations of the songpan earthquakes of august 1976 in sichuan, China. *J. Geophys. Res.* 89, 7697–7707. doi:10.1029/JB089iB09p07697
- Kirby, E., Harkins, N., Wang, E., Shi, X., Fan, C., and Burbank, D. (2007). Slip rate gradients along the eastern kunlun fault. *Tectonics* 26. doi:10.1029/2006TC002033
- Li, F., Liu, G., Jia, Q., Xu, X., Zhang, X., and Gong, F. (2018). Holocene active characteristics of the northern segment of the Minjiang fault in the eastern margin of the Tibetan plateau. *Seismol. Geol.* 01, 97–106. (in Chinese). doi:10.3969/j.issn.0253-4967.2018.01.008
- Li, J. (1988). Laminar and turbulent flow in the mammalian aorta: Reynolds number. *J. Theor. Biol.* 04, 409–414. (in Chinese). doi:10.1016/s0022-5193(88)80255-8
- Li, Z., Sun, J., Fang, L., Chen, X., Gao, M., Luo, Q., et al. (2021). Reproducing the spatial characteristics of high-frequency ground motions for the 1850 M7.5 xichang earthquake. *Seismol. Res. Lett.* 93, 100–117. doi:10.1785/0220210076
- Li, Z., Sun, J., Gao, M., Fu, G., An, Z., Zhao, Y., et al. (2022). Evaluation of horizontal ground motion waveforms at sedongpu glacier during the 2017 M6.9 mainling earthquake based on the equivalent green's function. *Eng. Geol.* 306, 106743. doi:10.1016/j.enggeo.2022.106743
- Long, F. (2008). *The velocity structure of the longmenshan fault zone and its neighborhoods and the focal mechanism solutions of the 2008 wenchuan earthquake sequence*. Hefei: University of Science and Technology of China. [dissertation/master's thesis]. [Hefei](in Chinese).
- Luo, Q., Dai, F., Liu, Y., and Chen, X. (2020). Simulating the near-field pulse-like ground motions of the imperial valley, California, earthquake. *Soil Dyn. Earthq. Eng.* 138, 106347. doi:10.1016/j.soildyn.2020.106347
- Mai, P. M., Imperatori, W., and Olsen, K. B. (2010). Erratum to hybrid broadband ground-motion simulations: Combining long-period deterministic synthetics with high-frequency multiple S-to-S backscattering. *Bull. Seismol. Soc. Am.* 100, 3338–3339. doi:10.1785/0120100283
- Miyake, H., Iwata, T., and Irikura, K. (2003). Source characterization for broadband ground-motion simulation: Kinematic heterogeneous source model and strong motion generation area. *Bull. Seismol. Soc. Am.* 93, 2531–2545. doi:10.1785/0120020183
- Morikawa, N., Senna, S., Hayakawa, Y., and Fujiwara, H. (2011). Shaking maps for scenario earthquakes by applying the development of the strong ground motion prediction method "recipe". *Pure Appl. Geophys.* 168, 645–657. doi:10.1007/s00024-010-0147-4
- Motazedian, D., and Atkinson, G. M. (2005). Stochastic Finite-Fault modeling based on a dynamic corner frequency. *Bull. Seismol. Soc. Am.* 95, 995–1010. doi:10.1785/0120030207
- Pitarka, A., Graves, R., Irikura, K., Miyake, H., and Rodgers, A. (2017). Performance of irikura recipe rupture model generator in earthquake ground motion simulations with graves and pitarka hybrid approach. *Pure Appl. Geophys.* 174, 3537–3555. doi:10.1007/s00024-017-1504-3
- Razafindrakoto, H. N. T., Bradley, B. A., and Graves, R. W. (2018). Broadband ground-motion simulation of the 2011 Mw 6.2 christchurch, New Zealand, earthquake. *Bull. Seismol. Soc. Am.* 108, 2130–2147. doi:10.1785/0120170388
- Roten, D., Olsen, K. B., and Pechmann, J. C. (2021). 3D simulations of M7 earthquakes on the Wasatch Fault, Utah, Part II: Broadband (0–10 Hz) ground motions and nonlinear soil behavior. *Bull. Seismol. Soc. Am.* 102, 2008–2030. doi:10.1785/0120110286
- Ripperger, J., Mai, P. M., and Ampuero, J.-P. (2008). Variability of near-field ground motion from dynamic earthquake rupture simulations. *Bull. Seismol. Soc. Am.* 98, 1207–1228. doi:10.1785/0120070076
- Schmedes, J., Archuleta, R. J., and Lavalle, D. (2010). Correlation of earthquake source parameters inferred from dynamic rupture simulations. *J. Geophys. Res.* 115, B03304. doi:10.1029/2009JB006689
- Somerville, P., Irikura, K., Graves, R., Sawada, S., Wald, D., Abrahamson, N., et al. (1999). Characterizing crustal earthquake slip models for the prediction of strong ground motion. *Seismol. Res. Lett.* 70, 59–80. doi:10.1785/gssrl.70.1.59
- Song, S. G. (2015). Developing a generalized pseudo-dynamic source model of Mw 6.5–7.0 to simulate strong ground motions. *Geophys. J. Int.* 204, 1254–1265. doi:10.1093/gji/ggv521
- Sørensen, M. B., Pulido, N., and Atakan, K. (2007). Sensitivity of ground-motion simulations to earthquake source parameters: A case study for istanbul, Turkey. *Bull. Seismol. Soc. Am.* 97, 881–900. doi:10.1785/0120060044
- Sun, J., Jin, X., Lin, J., Ma, Q., Zhang, L., Sun, B., et al. (2020). *The Chinese seismic intensity scale: GB/T17742-2020*. Beijing: China Earthquake Administration, 4–7. (in Chinese).
- Tang, R., and Liu, L. (1981). On the seismogeological characteristics of 1976 songpan-pingwu earthquakes. *Seismol. Geol.* 02, 41–86. (in Chinese).
- Wang, H. (2004). Finite fault source model for predicting near-field strong ground motion. *Institute of engineering mechanics*.
- Wang, H., Igel, H., Gallovič, F., Cochard, A., and Ewald, M. (2008). Source-related variations of ground motions in 3-D media: Application to the newport-inglewood fault, los angeles basin. *Geophys. J. Int.* 175 (1), 202–214. doi:10.1111/j.1365-246X.2008.03878.x
- Xu, X., Wen, X., Chen, G., and Yu, G. (2008). Discovery of the longriba fault zone in eastern bayan har block, China and its tectonic implication. *China Ser. D-Earth. Sci.* 05, 1209–1223. (in Chinese). doi:10.1007/s11430-008-0097-1
- Yao, H., Yang, Y., Wu, H., Zhang, P., and Wang, M. Crustal shear velocity model in Southwest China from joint seismological inversion CSES scientific products. (2019). doi:10.12093/02md.02.2018.01.v1
- Zeng, Y., Anderson, J. G., and Yu, G. (1994). A composite source model for computing realistic synthetic strong ground motions. *Geophys. Res. Lett.* 21, 725–728. doi:10.1029/94GL00367
- Zhao, X., Deng, Q., and Chen, S. (1994). Tectonic geomorphology of the Minshan uplift in Western Sichuan, southwestern China. *Seismol. Geol.* 04, 429–439. (in Chinese).
- Zhou, R., Li, Y., Alexander, L. D., Michael, A. E., He, Y., Wang, F., et al. (2006). Active tectonics of the eastern margin of the tibet plateau. *Mineralogy Petrology* 02, 40–51. (in Chinese). doi:10.19719/j.cnki.1001-6872.2006.02.007